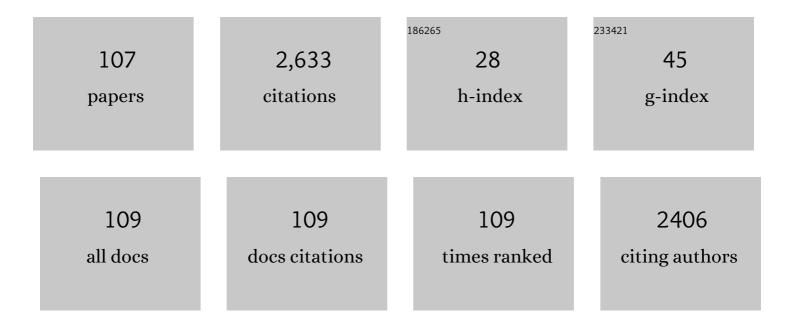
Siddheswar Maikap

List of Publications by Year in descending order

Source: https://exaly.com/author-pdf/6140365/publications.pdf Version: 2024-02-01



#	Article	IF	CITATIONS
1	Performance Improvement in E-Gun Deposited SiOx- Based RRAM Device by Switching Material Thickness Reduction. Journal of Physics: Conference Series, 2022, 2161, 012040.	0.4	1
2	Memristive and artificial synapse performance by using TiOx/Al2O3 interface engineering in MoS2-based metallic filament memory. Journal of Physics and Chemistry of Solids, 2021, 151, 109901.	4.0	16
3	Dopamine-Sensing Characteristics and Mechanism by Using N2/O2 Annealing in Pt/Ti/n-Si Structure. Electronics (Switzerland), 2021, 10, 3146.	3.1	1
4	Sensing characteristics of dopamine using Pt/n-Si structure. Vacuum, 2020, 172, 109050.	3.5	4
5	MoS ₂ based CBRAM with Mo/Ti barrier layer for artificial synapse application. , 2020, , .		1
6	Oxide-Electrolyte Thickness Dependence Diode-Like Threshold Switching and High on/off Ratio Characteristics by Using Al2O3 Based CBRAM. Electronics (Switzerland), 2020, 9, 1106.	3.1	8
7	Switching Characteristics and Mechanism Using Al2O3 Interfacial Layer in Al/Cu/GdOx/Al2O3/TiN Memristor. Electronics (Switzerland), 2020, 9, 1466.	3.1	9
8	Platinum membrane on Ti/n-Si substrate for dopamine detection. , 2020, , .		0
9	In Quest of Nonfilamentary Switching: A Synergistic Approach of Dual Nanostructure Engineering to Improve the Variability and Reliability of Resistive Randomâ€Accessâ€Memory Devices. Advanced Electronic Materials, 2020, 6, 2000209.	5.1	36
10	Sarcosine Prostate Cancer Biomarker Detection by Controlling Oxygen in NiO _{<i>x</i>} Membrane on Vertical Silicon Nanowires in Electrolyte–Insulator–Nanowire Structure. Analytical Chemistry, 2020, 92, 8064-8071.	6.5	18
11	Controlling Cu Migration on Resistive Switching, Artificial Synapse, and Glucose/Saliva Detection by Using an Optimized AlO <i>_x</i> Interfacial Layer in a-CO <i>_x</i> -Based Conductive Bridge Random Access Memory. ACS Omega, 2020, 5, 7032-7043.	3.5	30
12	Role of the Hf/Si Interfacial Layer on the High Performance of MoS ₂ -Based Conductive Bridge RAM for Artificial Synapse Application. IEEE Electron Device Letters, 2020, 41, 709-712.	3.9	33
13	Ru Conducting Filament Based Cross-Point Resistive Switching Memory for Future Low Power Operation. , 2020, , .		1
14	Resistive switching memory and artificial synapse by using Ti/MoS2 based conductive bridging cross-points. Vacuum, 2020, 176, 109326.	3.5	18
15	Controlling Conductive Filament and Tributyrin Sensing Using an Optimized Porous Iridium Interfacial Layer in Cu/Ir/TiN <i>_x</i> O <i>_y</i> /TiN. Advanced Electronic Materials, 2019, 5, 1800288.	5.1	30
16	Controlling Resistive Switching by Using an Optimized MoS ₂ Interfacial Layer and the Role of Top Electrodes on Ascorbic Acid Sensing in TaO <i>_x</i> -Based RRAM. Langmuir, 2019, 35, 3897-3906.	3.5	36
17	Evolution of resistive switching mechanism through H 2 O 2 sensing by using TaO x -based material in W/Al 2 O 3 /TaO x /TiN structure. Applied Surface Science, 2018, 433, 51-59.	6.1	27
	Prostate cancer biomarber detection by using Si nanowire based		

Prostate cancer biomarker detection by using Si nanowire based electrolyte/NiO<inf>x</inf>/SiO<inf>2</inf>/n-Si sensors., 2018,,.

#	Article	IF	CITATIONS
19	Cu Filament Based Resistive Switching and Oxidation Reduction through Dopamine Sensing in Novel Cu/MoS2/TinN Structure. , 2018, , .		1
20	Cross-Point Resistive Switching Memory and Urea Sensing by Using Annealed GdO _x Film in IrO _x /GdO _x /W Structure for Biomedical Applications. Journal of the Electrochemical Society, 2017, 164, B127-B135.	2.9	19
21	Understanding of multi-level resistive switching mechanism in GeOx through redox reaction in H2O2/sarcosine prostate cancer biomarker detection. Scientific Reports, 2017, 7, 11240.	3.3	27
22	Scalable cross-point resistive switching memory and mechanism through an understanding of H ₂ O ₂ /glucose sensing using an IrO _x /Al ₂ O ₃ /W structure. Physical Chemistry Chemical Physics, 2017, 19, 25938-25948.	2.8	21
23	Comparison of resistive switching characteristics by using e-gun/sputter deposited SiOx film in W/SiOx/TiN structure and pH/creatinine sensing through iridium electrode. Journal of Alloys and Compounds, 2017, 726, 30-40.	5.5	15
24	Effects of W/Ir Top Electrode on Resistive Switching and Dopamine Sensing by Using Optimized TaO <i>_x</i> â€Based Memory Platform. Advanced Materials Interfaces, 2017, 4, 1700959.	3.7	23
25	Negative voltage modulated multi-level resistive switching by using a Cr/BaTiOx/TiN structure and quantum conductance through evidence of H2O2 sensing mechanism. Scientific Reports, 2017, 7, 4735.	3.3	42
26	Highly Reliable Label-Free Detection of Urea/Glucose and Sensing Mechanism Using SiO2and CdSe-ZnS Nanoparticles in Electrolyte-Insulator-Semiconductor Structure. Journal of the Electrochemical Society, 2016, 163, B580-B587.	2.9	17
27	Evolution of complementary resistive switching characteristics using IrOx/GdOx/Al2O3/TiN structure. Applied Physics Letters, 2016, 108, .	3.3	54
28	Temperature-Dependent Non-linear Resistive Switching Characteristics and Mechanism Using a New W/WO3/WOx/W Structure. Nanoscale Research Letters, 2016, 11, 389.	5.7	43
29	Detection of pH and Enzyme-Free H2O2 Sensing Mechanism by Using GdO x Membrane in Electrolyte-Insulator-Semiconductor Structure. Nanoscale Research Letters, 2016, 11, 434.	5.7	6
30	Resistive and New Optical Switching Memory Characteristics Using Thermally Grown Ge0.2Se0.8 Film in Cu/GeSex/W Structure. Nanoscale Research Letters, 2015, 10, 392.	5.7	10
31	Conductive-bridging random access memory: challenges and opportunity for 3D architecture. Nanoscale Research Letters, 2015, 10, 188.	5.7	76
32	Observation of Resistive Switching Memory by Reducing Device Size in a New Cr/CrO x /TiO x /TiN Structure. Nano-Micro Letters, 2015, 7, 392-399.	27.0	24
33	Improved resistive switching phenomena and mechanism using Cu-Al alloy in a new Cu:AlOx/TaOx/TiN structure. Journal of Alloys and Compounds, 2015, 637, 517-523.	5.5	35
34	Energy band alignments of Al2O3–HfO2/Al2O3 nanolaminates–SiO2–p-type Si structures. Journal of Vacuum Science and Technology B:Nanotechnology and Microelectronics, 2015, 33, 051812.	1.2	5
35	Impact of device size and thickness of Al2O3 film on the Cu pillar and resistive switching characteristics for 3D cross-point memory application. Nanoscale Research Letters, 2014, 9, 692.	5.7	20
36	Impact of AlO <inf>x</inf> interfacial layer and switching mechanism in		2

W/AlO<inf>x</inf>/TaO<inf>x</inf>/TiN RRAMs., 2014, .

#	Article	IF	CITATIONS
37	Enhanced resistive switching memory characteristics and mechanism using a Ti nanolayer at the W/TaO x interface. Nanoscale Research Letters, 2014, 9, 125.	5.7	19
38	Enhanced resistive switching phenomena using low-positive-voltage format and self-compliance IrO x /GdO x /W cross-point memories. Nanoscale Research Letters, 2014, 9, 12.	5.7	30
39	Time-dependent pH sensing phenomena using CdSe/ZnS quantum dots in EIS structure. Nanoscale Research Letters, 2014, 9, 179.	5.7	17
40	Device Size-Dependent Improved Resistive Switching Memory Performance. IEEE Nanotechnology Magazine, 2014, 13, 409-417.	2.0	21
41	Self-compliance RRAM characteristics using a novel W/TaO x /TiN structure. Nanoscale Research Letters, 2014, 9, 292.	5.7	38
42	Copper pillar and memory characteristics using Al2O3 switching material for 3D architecture. Nanoscale Research Letters, 2014, 9, 366.	5.7	10
43	RRAM characteristics using a new Cr/GdOx/TiN structure. Nanoscale Research Letters, 2014, 9, 2404.	5.7	20
44	Resistive switching memory characteristics of Ge/GeO x nanowires and evidence of oxygen ion migration. Nanoscale Research Letters, 2013, 8, 220.	5.7	40
45	TaO x -based resistive switching memories: prospective and challenges. Nanoscale Research Letters, 2013, 8, 418.	5.7	170
46	Impact of electrically formed interfacial layer and improved memory characteristics of IrOx/high-l̂ºx/W structures containing AlOx, GdOx, HfOx, and TaOx switching materials. Nanoscale Research Letters, 2013, 8, 379.	5.7	23
47	Self-compliance-improved resistive switching using lr/TaO x /W cross-point memory. Nanoscale Research Letters, 2013, 8, 527.	5.7	24
48	Comparison of resistive switching characteristics using copper and aluminum electrodes on GeOx/W cross-point memories. Nanoscale Research Letters, 2013, 8, 509.	5.7	10
49	Nanocrystals for silicon-based light-emitting and memory devices. Journal Physics D: Applied Physics, 2013, 46, 153001.	2.8	95
50	Enhanced resistive switching memory characteristics and mechanism using a Ti nanolayer at the W/TaOx interface. Nanoscale Research Letters, 2013, 8, 288.	5.7	8
51	Bipolar Resistive Switching Memory Characteristics Using Al/Cu/GeO _x /W Memristor. ECS Transactions, 2012, 45, 257-261.	0.5	15
52	Record Resistance Ratio and Bipolar/Unipolar Resistive Switching Characteristics of Memory Device Using Germanium Oxide Solid Electrolyte. Japanese Journal of Applied Physics, 2012, 51, 04DD11.	1.5	7
53	Excellent Uniformity and Multilevel Operation in Formation-Free Low Power Resistive Switching Memory Using IrO\$_{x}\$/AIO\$_{x}/W Cross-Point. Japanese Journal of Applied Physics, 2012, 51, 04DD10.	1.5	9
54	Formation-Polarity-Dependent Improved Resistive Switching Memory Performance Using IrO\$_{x}\$/GdO\$_{x}\$/WO\$_{x}/W Structure. Japanese Journal of Applied Physics, 2012, 51, 04DD17.	1.5	7

#	Article	IF	CITATIONS
55	Bipolar resistive switching memory using bilayer TaOx/WOx films. Solid-State Electronics, 2012, 77, 35-40.	1.4	34
56	Improvement of Uniformity of Resistive Switching Parameters by Selecting the Electroformation Polarity in IrO _x /TaO _x /WO _x /W Structure. Japanese Journal of Applied Physics, 2012, 51, 04DD06.	1.5	7
57	Formation polarity dependent improved resistive switching memory characteristics using nanoscale (1.3 nm) core-shell IrOx nano-dots. Nanoscale Research Letters, 2012, 7, 194.	5.7	48
58	Excellent resistive memory characteristics and switching mechanism using a Ti nanolayer at the Cu/TaOx interface. Nanoscale Research Letters, 2012, 7, 345.	5.7	78
59	Enhanced nanoscale resistive switching memory characteristics and switching mechanism using high-Ge-content Ge0.5Se0.5 solid electrolyte. Nanoscale Research Letters, 2012, 7, 614.	5.7	29
60	Improvement of Uniformity of Resistive Switching Parameters by Selecting the Electroformation Polarity in IrO _{<i>x</i>} /TaO _{<i>x</i>} /WO _{<i>x</i>} /W Structure. Japanese Journal of Applied Physics, 2012, 51, 04DD06.	1.5	11
61	Excellent Uniformity and Multilevel Operation in Formation-Free Low Power Resistive Switching Memory Using IrO _{<i>x</i>/sub>/AlO_{<i>x</i>/sub>/W Cross-Point. Japanese Journal of Applied Physics, 2012, 51, 04DD10.}}	1.5	16
62	Record Resistance Ratio and Bipolar/Unipolar Resistive Switching Characteristics of Memory Device Using Germanium Oxide Solid Electrolyte. Japanese Journal of Applied Physics, 2012, 51, 04DD11.	1.5	3
63	Formation-Polarity-Dependent Improved Resistive Switching Memory Performance Using IrOx/GdOx/WOx/W Structure. Japanese Journal of Applied Physics, 2012, 51, 04DD17.	1.5	8
64	An observation of charge trapping phenomena in GaN/AlGaN/Gd <inf>2</inf> 0 <inf>3</inf> MOS schottky structure. , 2011, , .		0
65	High-κ Al ₂ O ₃ /WO _x Bilayer Dielectrics for Low-Power Resistive Switching Memory Applications. Japanese Journal of Applied Physics, 2011, 50, 10PH01.	1.5	21
66	Particle Size and Morphology of Iridium Oxide Nanocrystals in Non-Volatile Memory Device. Materials Transactions, 2011, 52, 331-335.	1.2	3
67	An observation of charge trapping phenomena in GaN/AlGaN/Gd2O3/Ni–Au structure. Applied Physics Letters, 2011, 98, .	3.3	14
68	Improved Resistive Switching Memory Characteristics Using Core-Shell IrO _x Nano-Dots in Al ₂ O ₃ /WO _x Bilayer Structure. Journal of the Electrochemical Society, 2011, 159, H177-H182.	2.9	34
69	High-κ Al ₂ O ₃ /WO _{<i>x</i>} Bilayer Dielectrics for Low-Power Resistive Switching Memory Applications. Japanese Journal of Applied Physics, 2011, 50, 10PH01.	1.5	13
70	Analysis of weakly bonded oxygen in HfO2/SiO2/Si stacks by using HRBS and ARXPS. Journal of Materials Science: Materials in Electronics, 2010, 21, 475-480.	2.2	17
71	Ruthenium oxide metal nanocrystal capacitors with high-κ dielectric tunneling barriers for nanoscale nonvolatile memory device applications. Microelectronic Engineering, 2010, 87, 1821-1827.	2.4	3
72	Low power resistive switching memory using Cu metallic filament in Ge0.2Se0.8 solid-electrolyte. Microelectronics Reliability, 2010, 50, 643-646.	1.7	12

#	Article	IF	CITATIONS
73	Characteristics of pH sensors fabricated by using protein-mediated CdSe/ZnS quantum dots. Microelectronics Reliability, 2010, 50, 747-752.	1.7	5
74	Improved Bipolar Resistive Switching Memory Using W/TaO _x /W Structure. Advanced Materials Research, 2010, 159, 333-337.	0.3	5
75	Bipolar Resistive Switching Memory Using Cu Metallic Filament in Ge[sub 0.4]Se[sub 0.6] Solid Electrolyte. Electrochemical and Solid-State Letters, 2010, 13, H159.	2.2	57
76	Physical and Memory Characteristics of Atomic-Layer-Deposited High-κ Hafnium–Aluminum-Oxide Nanocrystal Capacitors with Iridium-Oxide Metal Gate. Japanese Journal of Applied Physics, 2009, 48, 05DF02.	1.5	8
77	High-Î [®] HfO[sub 2] Nanocrystal Memory Capacitors Prepared by Phase Separation of Atomic-Layer-Deposited HfO[sub 2]â •Al[sub 2]O[sub 3] Nanomixtures. Journal of the Electrochemical Society, 2009, 156, K28.	2.9	28
78	Nanoscale (EOT = 5.6 nm) nonvolatile memory characteristics using n-Si/SiO ₂ <i>/</i> HfAlO nanocrystal/Al ₂ O ₃ <i>/</i> Ptcapacitors. Nanotechnology, 2008, 19, 435202.	2.6	29
79	Memory Characteristics of Atomic-Layer-Deposited High-κ HfAlO Nanocrystal Capacitors. Electrochemical and Solid-State Letters, 2008, 11, K50.	2.2	24
80	Low Voltage Operation of High-κ HfO ₂ /TiO ₂ /Al ₂ O ₃ Single Quantum Well for Nanoscale Flash Memory Device Applications. Japanese Journal of Applied Physics, 2008, 47, 1818.	1.5	10
81	TiO2Nanocrystal Prepared by Atomic-Layer-Deposition System for Non-Volatile Memory Application. Japanese Journal of Applied Physics, 2007, 46, 2523-2526.	1.5	7
82	Characteristics of strained-germanium p- and n-channel field effect transistors on a Si (1 1 1) substrate. Semiconductor Science and Technology, 2007, 22, 342-347.	2.0	28
83	HfO2/HfAlO/HfO2Nanolaminate Charge Trapping Layers for High-Performance Nonvolatile Memory Device Applications. Japanese Journal of Applied Physics, 2007, 46, 1803-1807.	1.5	11
84	Low-Power Switching of Nonvolatile Resistive Memory Using Hafnium Oxide. Japanese Journal of Applied Physics, 2007, 46, 2175-2179.	1.5	157
85	Charge storage characteristics of atomic layer deposited RuOx nanocrystals. Applied Physics Letters, 2007, 90, 253108.	3.3	41
86	Band offsets and charge storage characteristics of atomic layer deposited high-k HfO2â^•TiO2 multilayers. Applied Physics Letters, 2007, 90, 262901.	3.3	53
87	Charge trapping characteristics of atomic-layer-deposited HfO2 films with Al2O3 as a blocking oxide for high-density non-volatile memory device applications. Semiconductor Science and Technology, 2007, 22, 884-889.	2.0	124
88	Hole confinement at Si/SiGe heterojunction of strained-Si N and PMOS devices. Solid-State Electronics, 2006, 50, 109-113.	1.4	12
89	High-k gate oxide for silicon heterostructure MOSFET devices. Journal of Materials Science: Materials in Electronics, 2006, 17, 689-710.	2.2	25
90	MBE-grown high gate dielectrics of HfO2 and (Hf–Al)O2 for Si and Ill–V semiconductors nano-electronics. Journal of Crystal Growth, 2005, 278, 619-623.	1.5	26

#	Article	IF	CITATIONS
91	Effects of interfacial NH3/N2O-plasma treatment on the structural and electrical properties of ultra-thin HfO2 gate dielectrics on p-Si substrates. Solid-State Electronics, 2005, 49, 524-528.	1.4	22
92	Ultrathin oxynitride films grown on Si0.74Ge0.26/Si heterolayers using low energy plasma source nitrogen implantation. Solid-State Electronics, 2005, 49, 449-452.	1.4	9
93	Physical and reliability characteristics of Hf-based gate dielectrics on strained-Si/sub 1-x/Ge/sub x/ MOS devices. IEEE Transactions on Device and Materials Reliability, 2005, 5, 168-176.	2.0	7
94	Effect of strain on p-channel metal-oxide-semiconductor field-effect-transistor current enhancement using stress-modulated silicon nitride films. Applied Physics Letters, 2005, 87, 262109.	3.3	3
95	Mechanically Strained Strained-Si NMOSFETs. IEEE Electron Device Letters, 2004, 25, 40-42.	3.9	22
96	Charge storage and photoluminescence characteristics of silicon oxide embedded Ge nanocrystal trilayer structures. Applied Physics Letters, 2004, 84, 1386-1388.	3.3	59
97	Ge Outdiffusion Effect on Flicker Noise in Strained-Si nMOSFETs. IEEE Electron Device Letters, 2004, 25, 693-695.	3.9	56
98	Mechanically Strained Si–SiGe HBTs. IEEE Electron Device Letters, 2004, 25, 483-485.	3.9	16
99	Minority carrier lifetime and diffusion length in Si1â^'xâ^'yGexCy heterolayers. Solid-State Electronics, 2003, 47, 893-897.	1.4	10
100	Hafnium oxide gate dielectric for strained-Si1â^'xGex. Solid-State Electronics, 2003, 47, 1995-2000.	1.4	19
101	Interface properties and reliability of ultrathin oxynitride films grown on strained Si1â^'xGex substrates. Journal of Applied Physics, 2003, 93, 2464-2471.	2.5	12
102	Characteristics of ultrathin HfO2 gate dielectrics on strained-Si0.74Ge0.26 layers. Applied Physics Letters, 2003, 83, 779-781.	3.3	32
103	Electrical and interfacial characteristics of ultrathin ZrO2 gate dielectrics on strain compensated SiGeC/Si heterostructure. Applied Physics Letters, 2003, 82, 2320-2322.	3.3	41
104	Metal-oxide-semiconductor structure with Ge nanocrystals for memory devices applications. Electronics Letters, 2003, 39, 1865.	1.0	9
105	Series resistance and mobility degradation factor in C-incorporated SiGe heterostructure p-type metalÂoxide semiconductor field-effect transistors. Semiconductor Science and Technology, 2002, 17, 938-941.	2.0	12
106	Effects of nitric-oxide-plasma treatment on the electrical properties of tetraethylorthosilicate-deposited silicon dioxides on strained-Si[sub 1â°'x]Ge[sub x] layers. Applied Physics Letters, 2000, 77, 1840.	3.3	10
107	Growth of Silicon- Germanium Alloy Layers. Defence Science Journal, 2000, 50, 299-315.	0.8	7